AAS 03-066

# PRECISION POINTING FOR THE LASER INTERFEROMETRY SPACE ANTENNA MISSION

**T. T. Hyde, P. G. Maghami**
**NASA Goddard Space Flight Center**
**Guidance, Navigation and Control Division**
**Greenbelt, MD 20771**

## ABSTRACT

The Laser Interferometer Space Antenna (LISA) mission is a planned NASA-ESA gravitational wave detector consisting of three spacecraft in heliocentric orbit. Lasers are used to measure distance fluctuations between proof masses aboard each spacecraft to the picometer level over a 5 million kilometer separation. Each spacecraft and its two laser transmit/receive telescopes must be held stable in pointing to less than 8 nanoradians per root Hertz in the frequency band 0.1-100 mHz. The pointing error is sensed in the received beam and the spacecraft attitude is controlled with a set of micro-Newton thrusters. Requirements, sensors, actuators, control design, and simulations are described.

## THE LISA MISSION

The detection of gravity waves will open a new window of observation on the universe. Unlike typical observatories, which detect electromagnetic waves traveling through space-time, The Laser Interferometer Space Antenna (LISA) will detect ripples in space-time itself [1]. Science targets include galactic binaries, merging supermassive black holes, intermediate-mass/seed black holes, and cosmological backgrounds. Gravity waves are detected by measuring the strain in space, i.e. the change in distance between a set of masses separated a great distance. Ground based detection of gravity waves by LIGO and other observatories is possible with laser interferometry, but the relatively short arm length (4 km) and seismic noise limit the measurement band to above 10 Hz on the Earth. LISA also uses laser interferometeric measurement of the change in distance between test masses, but does it in space. Space allows very long arm lengths (5 million kilometers for LISA) and a very quiet acceleration environment ($3.5 \times 10^{-15}$ m/s$^2$/Hz$^{0.5}$ for LISA), which allows detection of gravity wave strains to a best sensitivity of $3 \times 10^{-24}$ strain and over the measurement band of $10^{-4}$ to $10^{-1}$ Hertz for a one year observation. Figure 1 shows a drawing of the LISA spacecraft with its Y-tube payload of two telescopes.

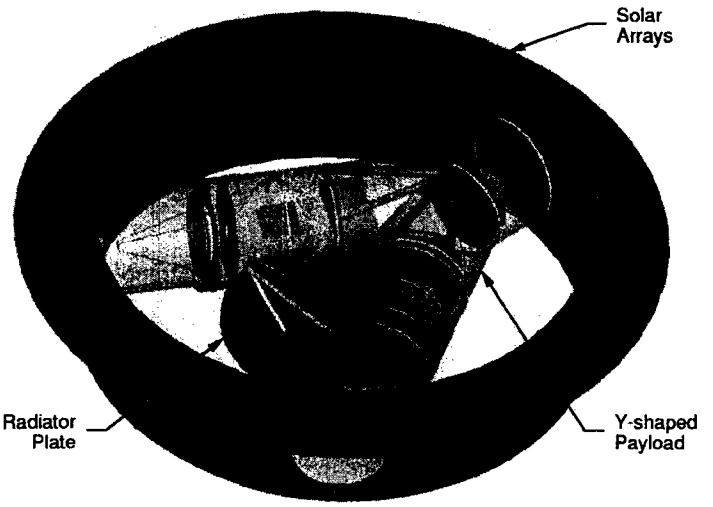


**Figure 1: The LISA Spacecraft**

The LISA mission consists of three spacecraft in heliocentric orbit. The orbits are chosen so that the three spacecraft form a roughly equilateral triangle with its center located at a radius of 1 AU and 20 degrees behind the Earth. Figure 2 shows how the LISA constellation triangle makes a "pin-wheel" motion about its center with a period of one year. The laser metrology arms between the three spacecraft are created by 1 watt, 1064 nm lasers that transmit through 30 cm aperture telescopes. Telescope diffraction creates a beam pattern about 40 km in diameter (first Airy ring) at the receive telescope which captures 70 picowatts of the laser power. The telescopes act in transmit and receive mode simultaneously, phase locking the return beam to enable the metrology in a way not unlike transponder based ranging for radio. The two telescopes on each spacecraft are mounted through a small articulation actuator that allows the angle between them to be slowly varied to cover the 59 to 61 degree range of triangle "breathing" created by the natural orbit dynamics.

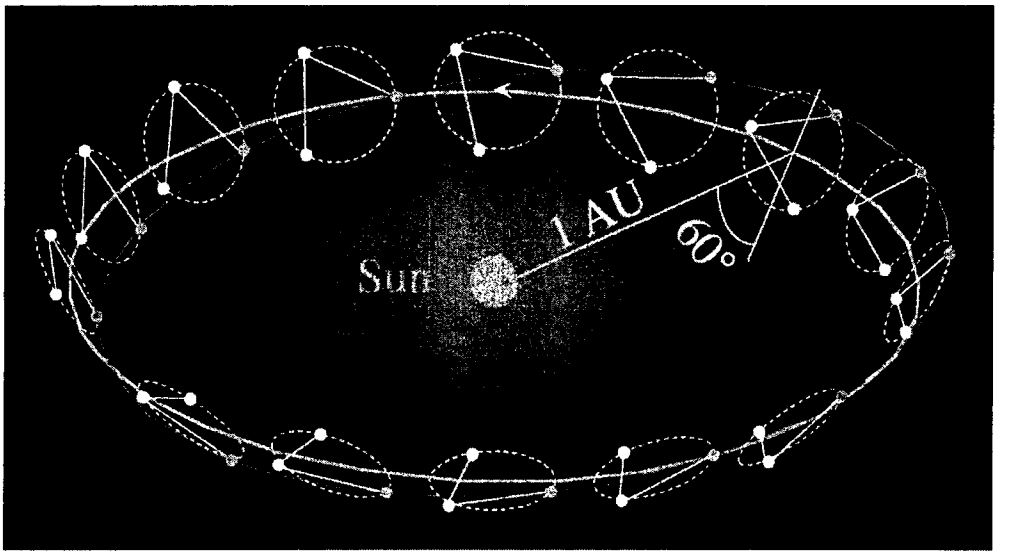


**Figure 2: The LISA Constellation**

The control system for LISA, called the Disturbance Reduction System (DRS), consists of five control functions:

1) Attitude control system (ACS): to orient the S/C to align the telescopes with incoming laser beams

2) Drag free control system (DFC): to maintain drag free motion of the proof masses in LISA measurement directions

3) Proof mass (PM) suspension control: to maintain relative attitude of the proof mass with respect to its housing and to maintain relative position of the proof mass with respect to its housing in the transverse directions

4) Telescope articulation (TA) control: to maintain the angle between the telescopes

5) Point ahead (PA) and acquisition control: to point the outgoing beam while sensing the incoming beam

LISA pointing is controlled through the closed loop ACS and open loop PA controls. The TA control may be open or closed loop depending on the mechanical impedance of the articulation actuator chosen. The proof mass displacement relative to its housing is measured in six degrees of freedom. This information is used to control the position of the spacecraft in translation to keep the proof mass centered in its housing and provide a drag free environment for the proof mass (DFC). A set of micro-Newton thrusters responds to the DFC force commands (in the three translation axes) and to the ACS torque commands (in the three rotation axes).

In order to realize the LISA design sensitivity very accurate laser metrology is required between the proof masses on the three LISA spacecraft. The change in distance measurement must be made with a noise level less than $4 \times 10^{-11}$ $m/Hz^{0.5}$ in the band 0.1-100 mHz. One contribution to this noise budget is that caused by the imperfections in the wavefront coupled with pointing jitter in the outgoing laser beam. The current budget allocation to pointing jitter is 8 nanoradian per root Hertz. This requires that spacecraft attitude also achieve this level since the telescopes are fixed to the spacecraft. This challenging pointing stability requirement is achieved through a unique set of sensors and actuators and straightforward single-input single-output (SISO) control loops.

## POINTING CONTROL

As in any control design task, the LISA pointing control is addressed with a good understanding of the plant, appropriate choice of sensors and actuators with the required range and resolution, and models of disturbance sources.

To understand the operation of LISA, one must "follow the light". The layout of the LISA optical bench is shown in Figure 3. The laser beam is launched from the fiber positioner and goes to the central polarizing beamsplitter (ps1). Most of the light (99%) is reflected at ps1 and goes out through the telescope into space. The received beam is collected by the telescope and comes onto the bench where a small amount (10%) is reflected by the beamsplitter (s1) and focused onto an acquisition CCD detector (marked qp2). The majority of the power (90%) goes through ps1 and to the proof mass. Upon reflection on the proof mass and return to ps1, the received beam is reflected, goes through the beam compressor (bc1), and onto the quadrant photodiode (qp1). Here it is mixed with the small amount (1%) of the outgoing laser in a heterodyne detection. The beat note is counted and the relative phase measured to better than $10^{-4}$ of a cycle to make the fundamental LISA measurement. The relative phase difference between the received and local wavefront on the four quadrant detectors is simultaneously used as the science mode pointing error sensor.

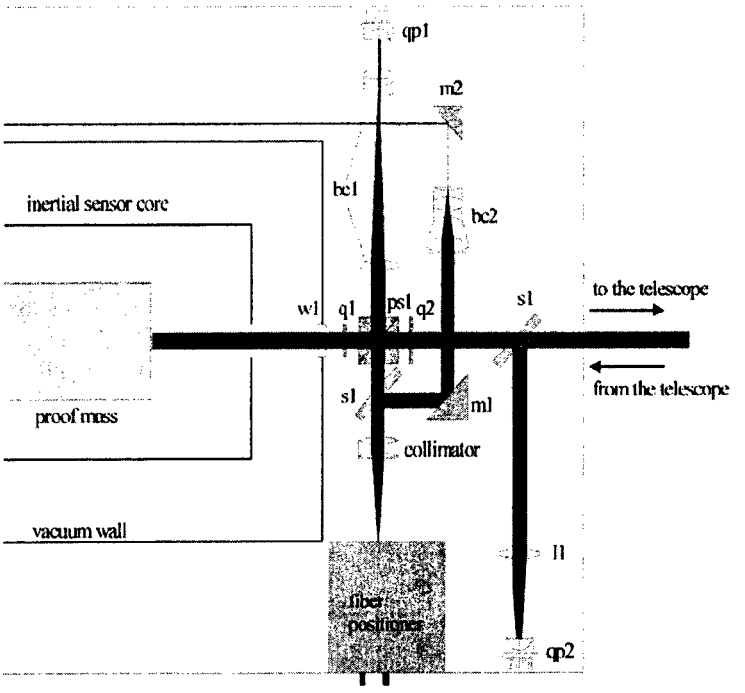


**Figure 3: Layout of the LISA Optical Bench**

A subtlety of the LISA transmit/receive configuration is the so-called "point ahead" angle required between the transmit and receive beam directions. The relative motion of the spacecraft and the finite speed of light requires that the beam be received from the location of the other spacecraft roughly 16 seconds ago and transmitted toward its location roughly 16 seconds in the future. Table 1 shows the magnitude of the fixed and time varying components of the point ahead angle. The point ahead compensation is handled by a commanded offset in the proof mass angle relative to the optics bench. Since the received beam bounces off the proof mass but the outgoing beam does not, the offset angle can be commanded open loop and scheduled on orbit dynamics.

**Table 1:**
**POINT AHEAD ANGLES**

| Component | Fixed | Time Varying |
|---|---|---|
| In-plane | 3.3 microrad | 55 nanorad |
| Out-of-plane | 85 nanorad | 5.8 microrad |

The sensors for LISA are unique among satellite control applications. Precision pointing error in science mode is computed from the relative phase error between the received beam and the local laser on the four quadrant detectors of qp1. This measurement is very close to the theoretical shot noise limit of:

$$NEA_{theoretical} = 1.22\,\lambda/DN^{0.5}$$

Where D is the telescope diameter of 30 cm, $\lambda$ is the wavelength of roughly 1 micron, and N is the photon count. In science mode, the received beam of 70 picowatts provides about 260 million detected photons (0.85 transmission ratio and QE of 0.70) over a 1 second integration. The $NEA_{theoretical}$ then is about 0.3 nanoradians. To be conservative and to account for other detector, background, and local laser shot noise sources, a value of 3 nanoradians per root Hertz is assumed for this science mode sensor. The two axis pointing errors from the two telescopes on the spacecraft are used to create a three axis attitude error quaternion. Other sensors include the displacement and attitude of proof mass relative to the housing measured with capacitive sensors, the acquisition CCD detectors (qp2), and two traditional star trackers. After acquisition (in science mode), the star trackers and CCDs are not used for fine pointing.

The actuators for LISA are also unique among satellite control applications. The spacecraft translation and orientation is controlled with a set of micro Newton thrusters. The baseline for these thrusters is a Field Emission Effect Propulsion (FEEP)[1] design that accelerates liquid metal ions with a voltage differential. The very high $I_{sp}$ mean that only a few grams of propellant are required for the entire mission. A minimum of six thrusters is required for six DOF control and twelve thrusters are provided for redundancy. Each thruster produces a linearly commandable force of up to 100 $\mu$N with a resolution of 0.1 $\mu$N. The other actuators are the telescope articulation actuators (1 degree stroke, 3 nanoradian resolution) and electrostatic forcers for six DOF proof mass control. Each telescope has an articulation actuator although only one is required (the other will be a cold spare). The electrostatic actuators use the same electrodes as the proof mass capacitive sensors.

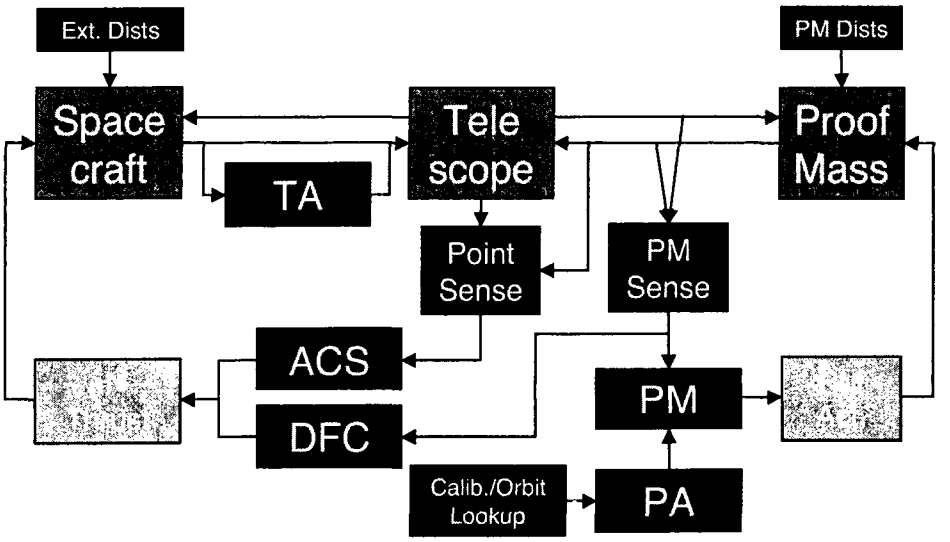


**Figure 4: LISA DRS Block Diagram (Control Functions are in Green)**

The LISA DRS control architecture is shown in the block diagram of Figure 4. During science mode, there are 16 sensor channels (2x2 pointing sensors, 2x6 proof mass sensors) and 19 actuator channels (6 thrusters, 2x6 proof mass actuators, 1 telescope articulator). Periodic calibration and orbit dynamics lookup provide an additional 4 point ahead values (2 axes for 2 telescopes). The multi input/multi output (MIMO) nature of the plant manifests in the coupling between the six axes within each proof mass sensor and actuator package, as well as between the proof mass and spacecraft coupled dynamics. However, straightforward SISO control of the individual pointing (ACS, 3 loops), drag free (DFC, 3 loops), and proof mass suspension (PM, 12 loops) feedback controls meets performance and robustness goals. This is due to the low coupling between controlled DOFs. The mass ratio between the proof mass (about 1.4 kg) and the spacecraft (over 300 kg) means that this coupling effect is relatively weak. The coupling in the proof mass electrodes is designed to be less than 1 percent between axes, meaning that this coupling effect is also relatively weak. Stability margins, acquisition operations, the 19 DOF model, and simulation results are described in the following sections.

## POINTING ACQUISITION

In order for LISA to accomplish pointing acquisition, a series of steps are taken. This process is initiated from ground command and then accomplished autonomously. First the two spacecraft point at each other based on star tracker measurements, and set their proof mass angles according to the required point ahead angles based on orbit dynamics. The outgoing beam on one spacecraft is spoiled to provide a 10 times wider angle (but 100 times dimmer) beam that encompasses the accuracy (noise and mounting bias) of the star tracker. The other spacecraft looks for the received beam in the acquisition CCD. The CCD measurement is then used to center the received beam on the detector qp1 with the local laser turned temporarily off. The received beam centroid is measured by qp1 in a direct detection quad cell mode (Direct QC). The local laser is turned on, and the heterodyne differential wavefront tilt measurement at qp1 is used. The other spacecraft repeats the process and finally both spacecraft return their beam to the focused condition. This allows detection of received beam angle at the full science mode sensitivity. Biases are calibrated at each step allowing re-acquisition to be accomplished without the direct QC step. An alternative acquisition scheme involves scanning over the uncertainty cone instead of spoiling the beam in the first step.

**Table 2**

**DYNAMIC RANGE ALLOCATIONS FOR ACQUISITION**

| Sensor | Resolution (1 Hz effective bandwidth) | Range | Alignment Bias to Next Sensor |
|---|---|---|---|
| Star Tracker | 5 microrad | Full sky | 20 microrad |
| CCD | 0.3 microrad | 360 microrad | 0.9 microrad |
| Direct QC | 30 nanorad | 3.6 microrad | 90 nanorad |
| Science Mode | 3 nanorad | 360 nanorad | N/A |

The allocation of requirements to the resolution, range and alignment bias allowed for each sensor in the acquisition process was done according to the following rule:

$$\text{Range}_{i+1} > 2\,(\,3\,\sigma_i + \text{Bias}_i\,)$$

That is, the range of the next sensor must encompass the accuracy (worst case bias plus three times the resolution) of the proceeding stage with 100 percent margin. Note that the bias from the direct QC to science mode is due to the potential misalignment of the local laser. Table 2 and Figure 5 show the requirements that have been allocated to the resolution, range, and alignment bias of each of the sensors used in the pointing acquisition process.

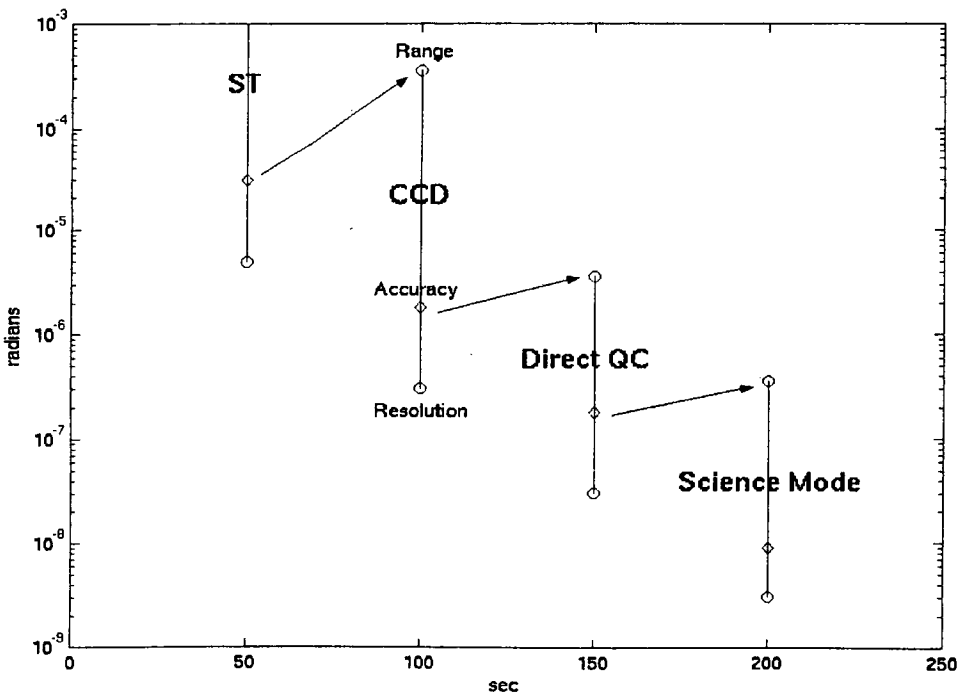


**Figure 5: Graphical Depiction of Sensor Range, Resolution, and Bias for Acquisition**

## THE 19 DOF MODEL

The LISA 19 DOF model [3] was developed to capture the dynamics of a typical LISA spacecraft in formation with two others. Dynamically, it includes all rigid-body degrees of freedom, six for the S/C translation and rotation; six for each proof mass translation and rotation; and finally one rotational DOF for telescope articulation. A number of disturbance sources, both internal and external, are included. Measurement noise for quad detector and capacitive sensing are included. The five control systems that comprise the LISA DRS are designed and included in the model. The dynamics of the LISA spacecraft is modeled and simulated in SIMULINK, a dynamic simulation tool. The configuration used for the current 19-DOF Model is shown in Figure 6.

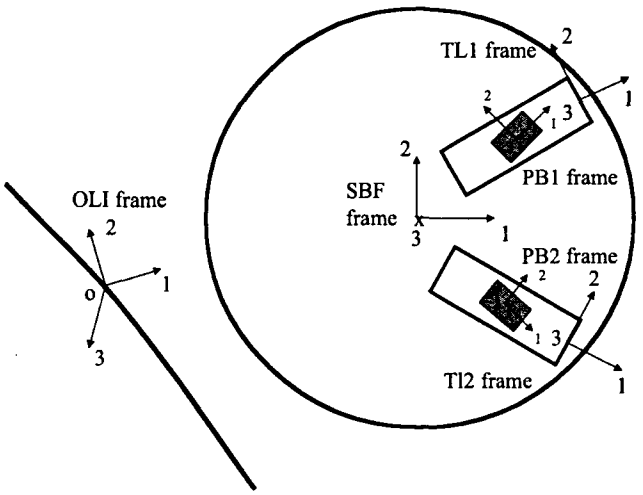


**Figure 6: 19 DOF Model Configuration**

White-noise models were used to capture thruster force, electrostatic suspension force, capacitive sensor, star tracker, CCD, direct quad cell, and science mode pointing sensor. The intensity levels used are given in Table 3. Colored noise models were used for the solar radiation flux variations (Figure 7), and for the proof mass acceleration variations (Figure 8). This solar variation spectrum is based on refs. [1] and [2], and represents a conservative assessment of potential variations. This spectrum includes the so-called 5-minute acoustic oscillation. The proof mass acceleration noise includes a number of sources including magnetic and Lorentz forces, thermal disturbances, cosmic ray impacts, etc [2].

**Table 3:**
**ACTUATION AND SENSING NOISE INTENSITIES**

| Noise Source | Intensity |
|---|---|
| Thrusters | 0.1 $\mu N/Hz^{0.5}$ |
| Suspension Force | 2e-14 $N/Hz^{0.5}$ |
| Capacitive Sensing | 3 $nm/Hz^{0.5}$ |
| Star Tracker | 5 $microrad/Hz^{0.5}$ |
| CCD | 0.3 $microrad/Hz^{0.5}$ |
| Direct QC | 30 $nanorad/Hz^{0.5}$ |
| Science Mode | 3 $nrad/Hz^{0.5}$ |

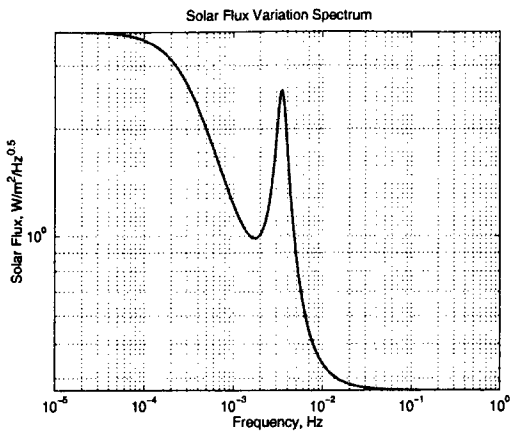


**Figure 7: Root Power Spectrum of the Solar Radiation Flux Variations**

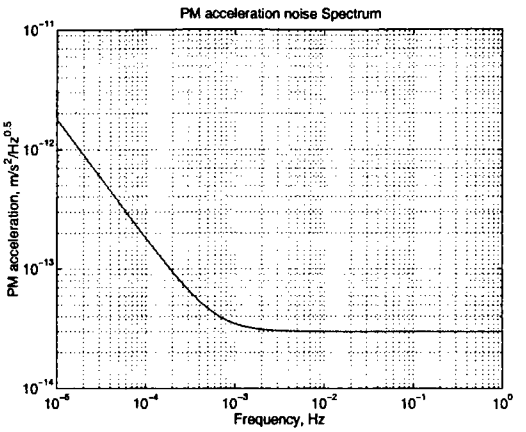


**Figure 8: Root Power Spectrum for the Proof Mass Acceleration Variations**

## STABILITY MARGINS

Each of the controllers was designed to have sufficient stability margins. However the 19-DOF system represented in Figure 1 is a MIMO system, by virtue of the cross coupling between the relative test mass positions and the attitude of the spacecraft. Hence, the loop gains at each input and output channel (while the remaining channels are closed) must be analyzed to obtain proper stability margins. The stability analysis indicates that each input/output channel meets the requirements of at least 9 dB of gain margin and 35° of phase margin. These margins are amply sufficient considering that the effects of zero-order hold and computational and transport delays are already included in the analysis. Figure 9 illustrates the loop gain for one of the pointing axes loops.

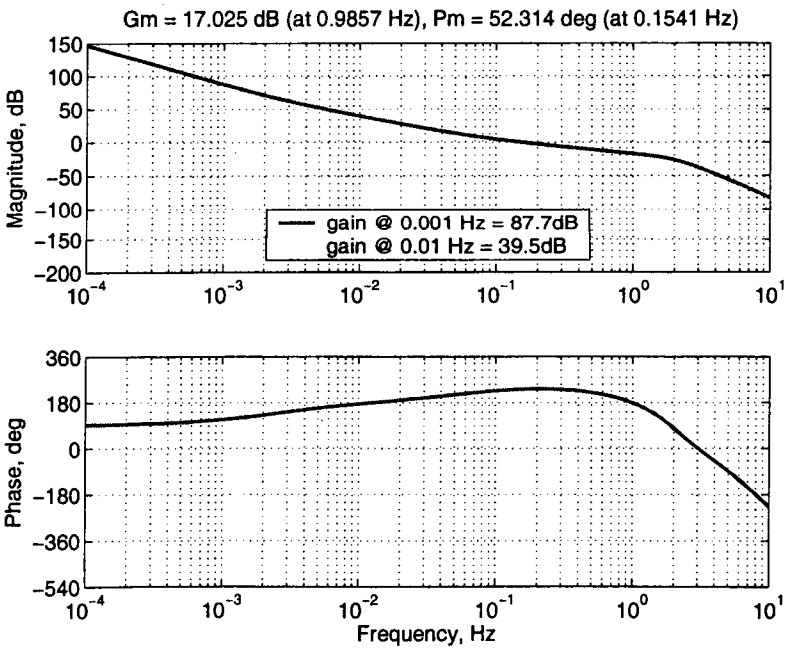


**Figure 9: Gain and Phase Margins for one of the LISA Pointing Loops.**

## SIMULATION RESULTS

A time domain simulation was run for 1000 seconds. In order to see the effect of pointing acquisition operations, a sequence of sensors was "turned on". Table 4 lists these transitions. The bias error for each sensor was set according to its maximum allotment (see Table 2).

**Table 4:**
**SENSOR MODE TRANSITIONS DURING SIMULATION**

| Simulation time (seconds) | Pointing sensor mode |
|---|---|
| 0 | Star trackers only on |
| 250 | CCD turned on |
| 500 | Direct QC turned on |
| 750 | Science mode pointing turned on |

Figure 10 shows the two axis pointing error for telescope 1 throughout the acquisition process. With star tracker only on (0-250 seconds), the pointing error is consistent with the alignment bias and noise of the star tracker. At t=250 seconds, the CCD is used, resulting in a transient to a new steady state condition (Figure 11). Here the pointing error is consistent with the bias and noise of the CCD sensor. At t=500 seconds, the quadrant detector is used in direct detection mode (Direct QC), resulting in another transient to a third steady state condition (Figure 12). Here the pointing error is consistent with the bias and noise of the direct QC sensor. Finally, the local laser is turned on, the received beam has been focused, and the science mode sensor therefore enabled. Figure 13 shows the final, post-acquisition, performance of just over 1 nanoradian rms.

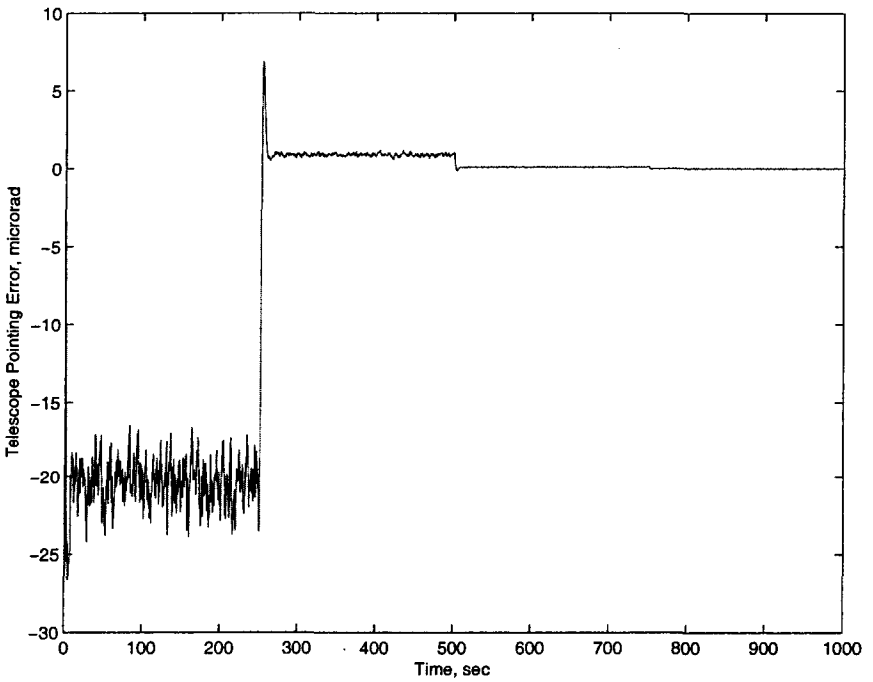


**Figure 10: Beam Pointing Error throughout Acquisition**

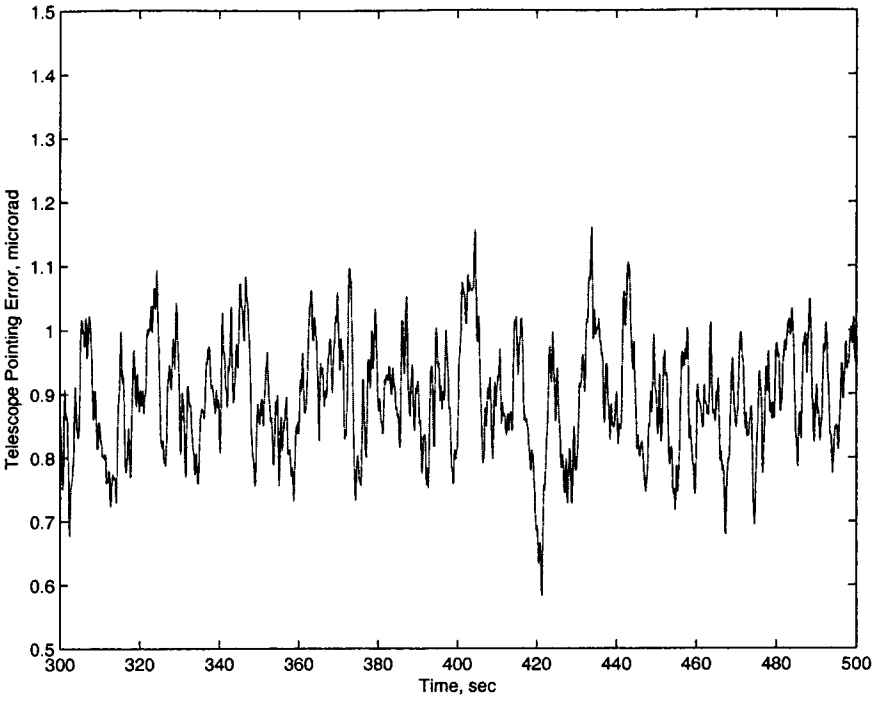


**Figure 11: Beam Pointing Error in CCD Mode**

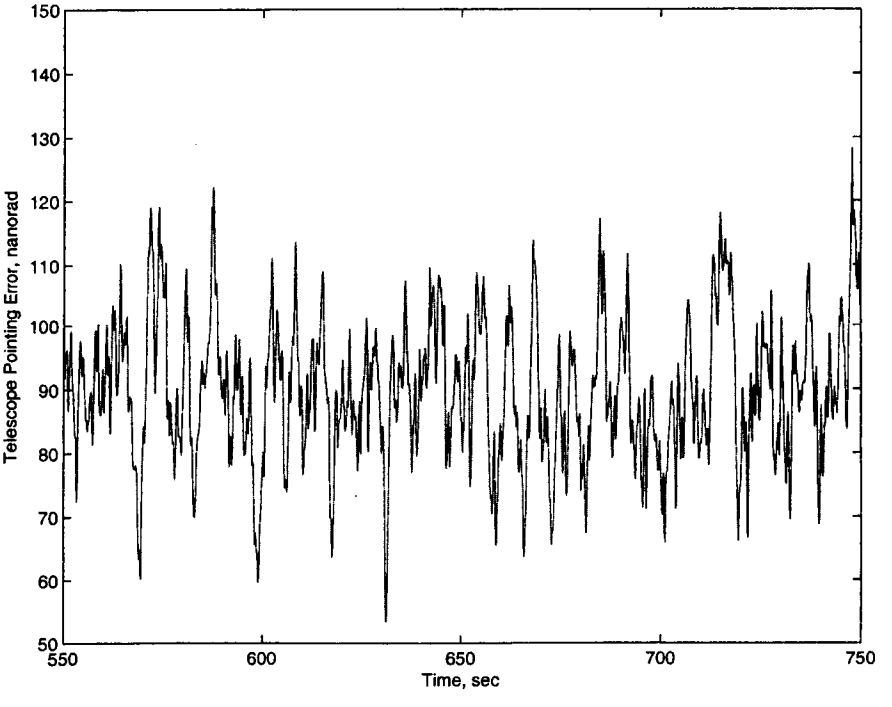


**Figure 12: Beam Pointing Error in Direct Quad Cell Mode**

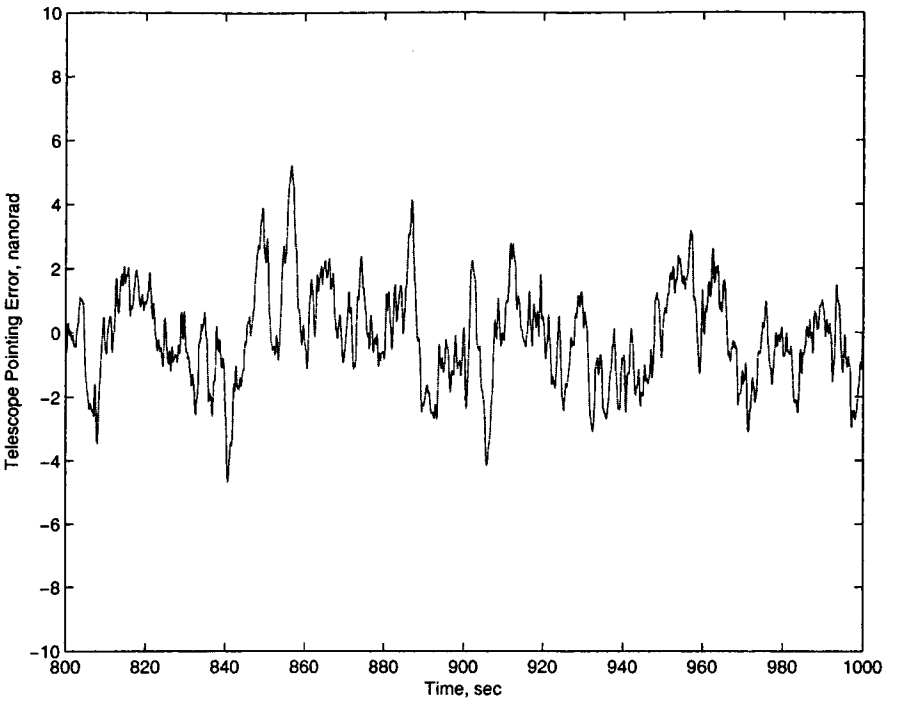


**Figure 13: Beam Pointing Error in Science Mode.**

The science mode pointing error shown in Figure 13 has an rms of just over 1 nanoradian. This value (0.0002 arcsec) is more than an order of magnitude lower than any spacecraft pointing control system to date. The Hubble Space Telescope pointing performance is about 0.004 arcsec. It is LISA's unique sensor based on received laser wavefront that allows this level of pointing performance. The low force noise micro-Newton thrusters and the low disturbance spacecraft are also consistent with achieving this unprecedented spacecraft pointing performance.

The performance requirement for LISA pointing is specified in variation power over the frequency range of 0.1-100 mHz, so a longer simulation is science mode was run and the spectrum taken. Figure 14 shows the root power spectral density for the pointing error of telescope 1 in two axes. The peak level of about 3 nanoradians per root Hertz meets the requirement of 8 nanoradians per root Hertz with over 100 percent margin.

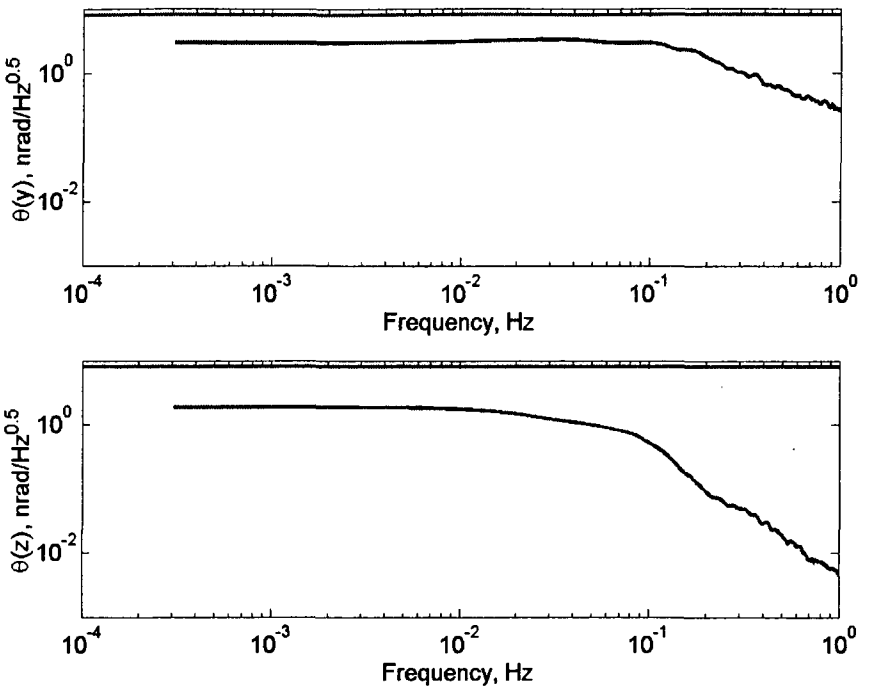


**Figure 13: Root PSD of Pointing Error in Science Mode.**

## CONCLUSIONS

The precision pointing performance for LISA has been shown through detailed time domain simulation. Science mode pointing stability of a little over 1 nanoradian RMS is an order of magnitude better than any spacecraft known. This is accomplished due to LISA's unique pointing error sensor that uses the received beam wavefront tilt and precision phase measurement on four quadrants. The predicted level of less than 4 nanoradian/$Hz^{0.5}$ in the LISA measurement bandwidth proves significant performance margin to the 8 nanoradian/$Hz^{0.5}$ requirement. The control laws have shown to be robust through traditional frequency domain analysis. The acquisition scenario has been shown to work with successive layers of sensor precision. The dynamic range of each sensor encompasses the accuracy and bias in the preceding layer with appropriate margins. Time domain simulation of the acquisition process that shows no special control mode changes are required and that science mode lock can be achieved in the budgeted time allotment.

## REFERENCES

[1] *Final Technical Report of the (Phase A) Study of the Laser Interferometer Space Antenna* (Dornier Satellitensysteme GmbH - Matra Marconi Space - Alenia Aerospazio), ESTEC Contract no. 13631/99/NL/MS, Report No. LI-RP-DS-009 (April 2000). Available via anonymous ftp at ftp.estec.esa.nl in directory pub/sci-spd/lisa/LISA Documents.

[2] J. Pap, et. al., "Variation in Total Solar and Spectral Irradiance as Measured by the VIRGO Experiment on SOHO", *Adv. Space Res.*, 24:215-224, 1999.

[3] P. Maghami, and T. Hyde, "Laser Interferometer Space Antenna 19-DOF Controls Model," to appear in the Journal of Classical and Quantum Physics, 2003.